Temperature Anomalies in the Northeastern North Atlantic: Subpolar and Subtropical Precursors on Multiannual Time Scales

MARTINA M. JUNGE AND KLAUS FRAEDRICH

Meteorologisches Institut, Universität Hamburg, Hamburg, Germany

(Manuscript received 20 December 2005, in final form 19 June 2006)

ABSTRACT

An adjoint ocean general circulation model of the North Atlantic is employed to calculate sensitivities of temperature in the northeastern North Atlantic with respect to atmospheric nonlocal fluxes and ocean state variables at prior times, up to 7 yr.

Maximum sensitivities cross the Atlantic from east to west within 3 to 4 yr. On this interannual time scale, advection of temperature perturbations by the climatological flow is suggested as the prime mechanism responsible for SST perturbations in the northeastern North Atlantic. The pathway of sensitivities lies preferentially beneath the surface and can be understood in terms of the reemergence mechanism. This provides the link between local forcing, mainly by heat flux in winter, and resurfacing of perturbations at remote locations.

On the multiannual to decadal time scale, the western subpolar gyre plays a key role: negative temperature sensitivities that evolve in parallel with positive salinity sensitivities in the Labrador and Irminger Seas give rise to pressure gradients and velocity perturbations that have effects on SST by modifying the oceanic heat transport into the northeastern North Atlantic. Together with additional influence from the Tropics and the subtropical gyre on time scales of 5 yr and beyond, these sensitivities combine to make a plethora of time scales that play a role in shaping SST perturbations in the North Atlantic.

1. Introduction

Prediction of European climate beyond the time scale of traveling weather systems has been a recurrent theme of climate research for many decades. Various authors have published research that ties long-term predictability of European climate to predictability of SST near Europe, or more generally along the North Atlantic Current (NAC; Czaja and Frankignoul 1999; Marshall et al. 2001). Fraedrich et al. (2004) identify the northeastern North Atlantic as a region characterized by long-term memory in SST variability indicated by a $1/f$ power-law scaling in the low-frequency part of the spectrum, a result prevalent in both models and observations (Fraedrich and Blender 2003). On the interannual time scale the dominant characteristic of SST anomalies in the North Atlantic is the tripole pattern, and many investigators have demonstrated that this is predominantly forced by atmospheric fluxes (Frankignoul 1985; Deser and Blackmon 1993). This means that there is effectively very little potential for predictability of the *local* atmosphere from *local* SST anomalies. On decadal time scales, results by Hansen and Bezdek (1996) and Sutton and Allen (1997) suggest large-scale propagation of SST anomalies along the North Atlantic Current. According to Krahmann et al. (2001), the propagation speed might be determined by the prevailing frequency of the North Atlantic Oscillation (NAO), which entails a particular heat flux forcing pattern that reinforces or damps anomalies along the path in different phases of their translation.

More recently Shina et al. (2004) found SST anomaly propagation along the Gulf Stream and the North Atlantic Current also on the shorter interannual time scale in a 1000-yr coupled model integration, but the authors could not confirm the existence of such SST propagations in observations. The model integration, however, did also show occurrences of the larger-scale, slower-propagating decadal fluctuations with similar characteristics as had been analyzed by Hansen and Bezdek (1996) and Sutton and Allen (1997). While the physical

Corresponding author address: Martina M. Junge, Meteorologisches Institut, Universität Hamburg, Bundesstrasse 55, 20146 Hamburg, Germany.
E-mail: martina.junge@zmaw.de

DOI: 10.1175/JCLI4078.1

mechanism in the model anomaly propagation on the interannual time scale is unambiguously identified as advection of thermal anomalies by the mean currents, a convincing explanation of the decadal wandering of SST excursions in either observations or models has yet to be established. From the analysis of the Third Hadley Centre Coupled Ocean–Atmosphere GCM (HadCM3) model [the same as was investigated by Shina et al. (2004)] Cooper and Gordon (2002) conclude that strong convection in the Labrador Sea can cause changes in the velocity and orientation of the NAC through a thickening of the Labrador Sea Water layer in almost the entire subpolar gyre, and thus give rise to changes in pressure gradients and hence to these velocity perturbations. The consequence of these changes is an increased heat transport to the north and, therefore, variations of SST on the decadal time scale. The thickening of Labrador Sea Water propagating through the North Atlantic as Upper North Atlantic Deep Water has also been shown for observational data by Curry and McCartney (2001).

Our aim here is to try and disentangle some of the physical/dynamical mechanisms that work together to produce SST anomalies in the eastern North Atlantic. The tool is an adjoint ocean model. Our approach is an inverse one. Instead of integrating models and examining any potential SST propagations that display some resemblance with results from observations, we *assume* changes in SST or ocean heat content in the eastern North Atlantic and ask the question: which perturbations of model variables do have the potential to cause these changes? The adjoint model we are employing propagates these sensitivities backward in time and thus draws spatial pictures showing the evolution of the influential regions with time.

Section 2 introduces the ocean model and its adjoint, including the experimental setup. Section 3 contains the experiment results. In section 4 we discuss these results in light of time scales and possible mechanisms involved and conclude with a short summary of the new aspects put forward in this paper.

2. Model and experimental setup

a. The ocean model

The ocean model used for this study is the North Atlantic version of the Hamburg Ocean Primitive Equation (HOPE) model (Wolff et al. 1997). The domain covers 40°S–80°N, 100°W–20°E. The prognostic variables are the three-dimensional velocity field, temperature, salinity, and sea surface elevation. The grid points are organized on an Arakawa E-grid, which is a staggered composition of two grids overlaying each other in such a way that the "even" mesh is shifted half a grid step in both the eastern and northern direction in relation to the "odd" mesh. The resolution of each of these grids is 1.4° in latitude and longitude with 20 levels in the vertical (the upper 10 levels represent the upper 300 m of the water column). Realistic topography and coastline are implemented within the limitation of the resolution. At the northern and southern boundaries temperature and salinity are relaxed toward the Levitus (1982) climatology over the whole water column. The Mediterranean outflow is parameterized, and a constant climatological distribution of sea ice is applied. Linearly interpolated climatological monthly mean fields of atmospheric fluxes have been used to force the model. The forcing fields are derived from the Hellermann and Rosenstein (1983) wind stress, Esbensen and Kushnir (1981) heat fluxes and solar radiation, and Jaeger (1976) precipitation minus Esbensen and Kushnir (1981) evaporation fields. In ice-free areas surface temperature T is relaxed toward the Levitus (1982) climatology T_{clim} such that the restoring heat flux is given by $\lambda(T–T_{\mathrm{clim}})$, where λ is 40 (W m^{-2}) °C^{-1}. This heat flux implies a time scale for relaxation of SST anomalies, and hence of sensitivity, of about two months (for a water column 40 m deep). A similar relaxation is applied to sea surface salinity with a time scale of 30 days. These forcing fields drive an annual cycle that is designed to capture the main features of North Atlantic seasonal climatology.

These forcing fields do not include stochastic forcing, which is undoubtedly of relevance for the variability of the gyre circulation (Frankignoul et al. 1997) and thus changes in the ocean heat content. Development and application of a hybrid coupled model that incorporates stochastic forcing in all the air–sea fluxes and the feedback from the ocean, together with its adjoint, are under way (S. Osprey 2005, personal communication). The application of the coupled model to the questions posed in this manuscript will build upon the results described here. Thus, we consider the experiments with the climatological forcing used here as a benchmark also for the coupled experiments.

b. Adjoint sensitivity analysis and experimental setup

The North Atlantic HOPE model has previously been used for an adjoint sensitivity study of SST anomalies on the North Atlantic tripole centers, and details on the interpretation of adjoint sensitivities are described in Junge and Haine (2001), together with the adjoint code. Adjoint sensitivity analysis has also been explained, for example, in Errico (1997).

The adjoint evolves from the definition of the response function J as an inner product, for example, the area averaged heat content in a particular area. Posing the question of how sensitive this response function proves to initial or boundary conditions leads to the tangent-linear system that describes how a (small) perturbation in the basic state evolves with time. With the adjoint of the tangent-linear system the gradients $\partial J/\partial x_i(t)$ can be calculated, with x_i (t) representing any prognostic ocean model variable or forcing at some grid point i at any time t prior to the calculation of J. These adjoint sensitivities are thus derived from the model equations and hence are dynamically based, not statistical. The derivation from the tangent-linear model implies that the solutions are only valid for small perturbations of the background state.

To calculate sensitivities of northeast Atlantic temperature with the adjoint model, the definition of a response function J as a forcing to the adjoint is taken as averaging operator in space and time, namely, 12-month averages in the area 50°–60°N, 10°–20°W west of Scotland, subsequently named the *target area*. The selection of this region is motivated by results of Sutton and Allen (1997) showing high correlations of SST anomalies in this area with SST anomalies near Cape Hatteras, North Carolina, 7 yr earlier.

Two slightly differing definitions of the response function J are used for a set of two experiments:

$$J_{\mathrm{T300}} \equiv \left\langle \frac{1}{H} \int_{z=0}^{z=H} T(z)\, dz \right\rangle_{t,\mathrm{space}}, \qquad (1)$$

with $H = 300$ m, and

$$J_{\mathrm{SST}} \equiv \langle T(z = 5 \quad \mathrm{m}) \rangle_{t,\mathrm{space}}, \qquad (2)$$

with $z = 5$ m being the midpoint of the first model layer, that is, taken as representative of SST, and $\langle \cdot \rangle_{t,\mathrm{space}}$ denoting the annual mean of temperature T, averaged over the target area.

The mixed layer in the target area reaches a depth of 400–500 m in winter. Taking the vertical average of temperature [Eq. (1)] over the upper 300 m provides a direct forcing for the thermocline waters in the adjoint calculation. On the other hand, taking only SST [Eq. (2)], this connection has to be established first by vertical mixing through turbulent fluxes before sensitivities can be traced below the surface. Comparing the sensitivities of these two experiments will give us some guidance as to how effective the subsurface waters are for providing a memory for SST perturbations.

The forward model has been integrated over 40 yr with climatological forcing, and the adjoint calculations are then derived for 8 yr, going back in time. Sensitivities of the respective response function J are calculated with respect to (w.r.t.) the prognostic ocean state variables (temperature, salinity, velocity, and sea surface elevation) and surface forcing at all prior times during the preceding eight years. Thus, by performing the adjoint calculation, we obtain a description of the sensitivity of heat content or SST over an 8-yr period that is space and time dependent.

The output of the adjoint calculations, that is, the sensitivity values, are representative for the box volume of each grid point. As the volume increases, for example, with depth, the sensitivities have to be normalized. The way this is done here is to set the weighting coefficient to 1 for a surface grid box in the center of the target area and to derive weighting coefficients for every grid box as volume divided by this standardized gridbox volume. Note that this is a purely diagnostic procedure, applied after the model integration for display purposes.

3. Results

a. North Atlantic Current and subpolar precursors

The purpose of the experiment design is to reveal—within this model world—which quantities influence SST and heat content in the eastern North Atlantic: what is their spatial extent, what is their temporal evolution, which are the relevant time scales, and how do different processes work together to make up what we observe in the northeastern corner of the North Atlantic?

Figure 1 displays annually averaged sensitivities of J_{T300} w.r.t. temperature at 300-m depths and Fig. 2 the same quantity w.r.t. temperature at the ocean surface for up to seven years prior to the calculation of J_{T300}. The notion of the year numbers is such that year -1 is one year, that is, 13 to 24 months prior to the calculation of J_{T300}, year -2 is two years, that is, 25 to 36 months prior to the calculation of J_{T300}, and so forth. Year 0 is the year over which the response function J_{T300} is averaged.

Considering sensitivities at 300-m depth first, year -1 (Fig. 1a) and year -2 (Fig. 1b) show that the sensitivity w.r.t. temperature perturbations is essentially confined to the path of the North Atlantic Current in the model. The sign of the sensitivities is such that positive perturbations of temperature lead to positive perturbations of J_{T300}, and thus heat content in the target area 2 to 3 yr later. In year -2 prior to the calculation of J_{T300} the fastest propagating signal has already reached the U.S. East Coast, though the maximum signal is still anchored somewhere between 40° and 60°W. In year -3 the sensitivities have reached the U.S. coast and the Gulf Stream area. Thus the time scale of the

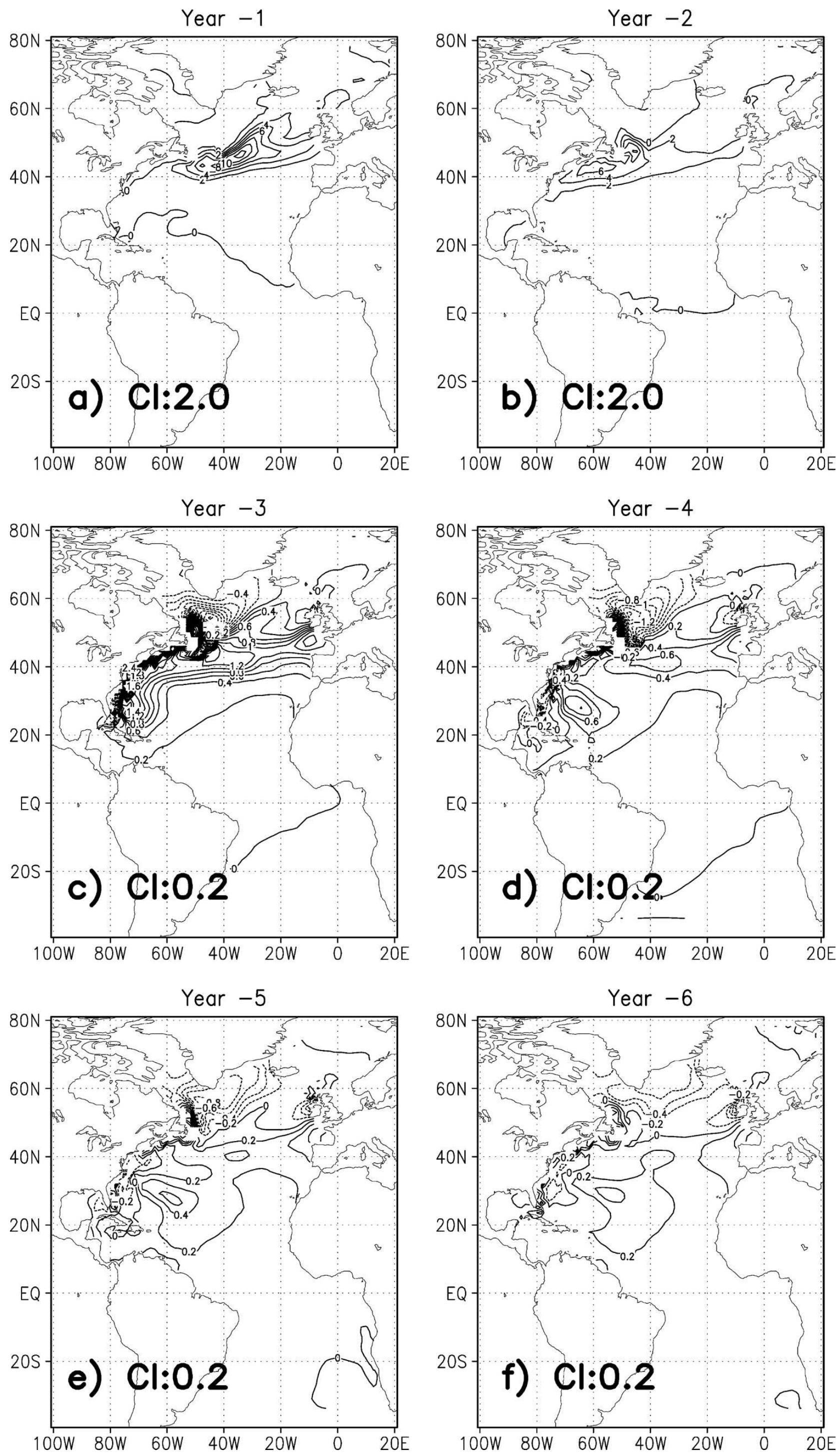

FIG. 1. Annual average of sensitivity of J_{T300} w.r.t. temperature at 300-m depth for years (a) −1, (b) −2, (c) −3, (d) −4, (e) −5, and (f) −6 prior to the calculation of J_{T300}. Contour interval (CI): 2.0×10^{-5} for (a) and (b), and 0.2×10^{-5} for (c)–(d).

highest sensitivities to cross the North Atlantic is on the order of 3 to 4 yr.

The mechanism by which this propagation can most likely be explained is the advection of temperature perturbations by the mean currents. The distance from the U.S. coast to the target area off the British Isles amounts to roughly 6000 km. Velocities at 300 m along this path vary from 25 to 2 cm s^{-1} (with about 10%

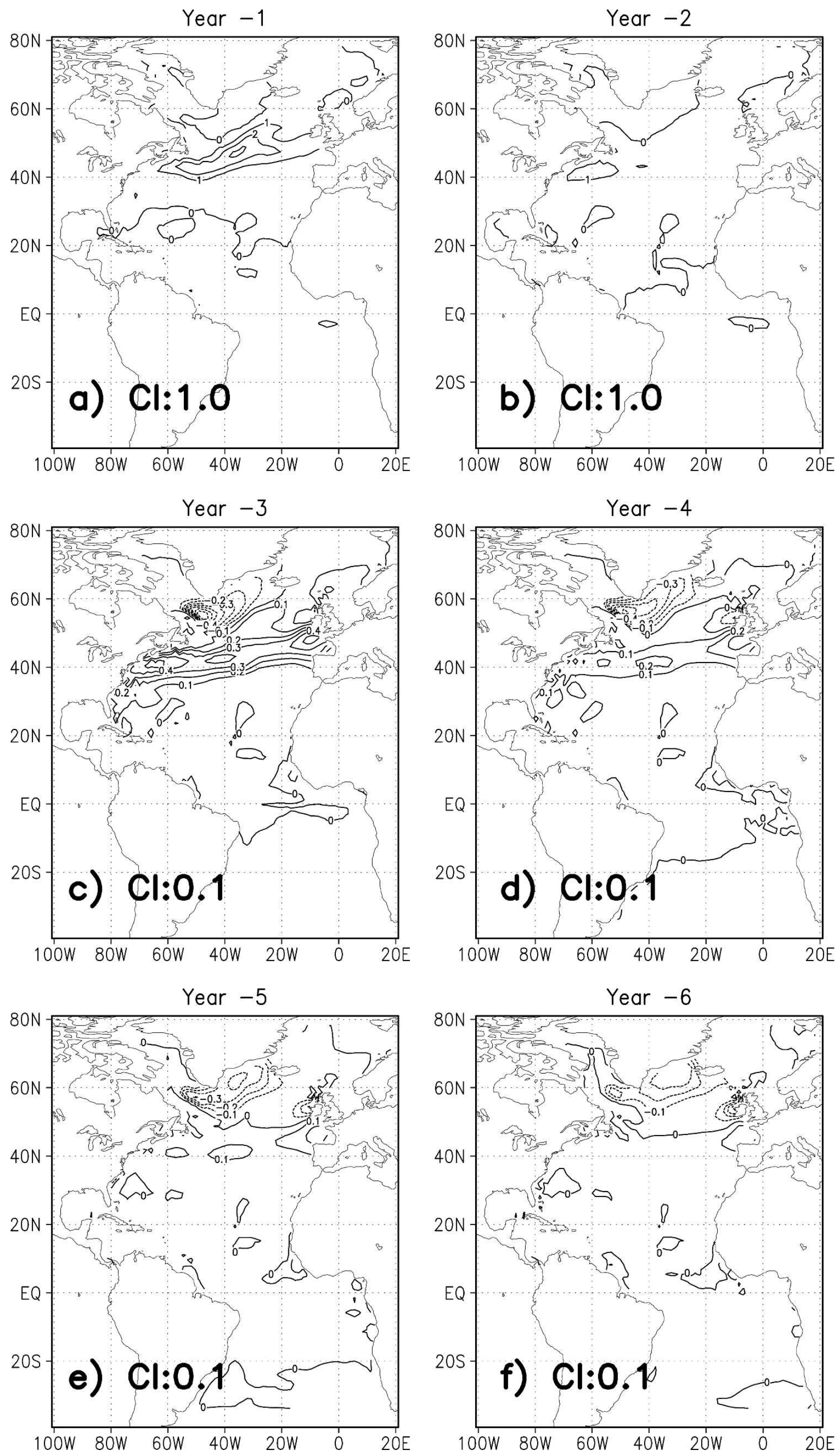

FIG. 2. Same as in Fig. 1, but w.r.t. sea surface temperature. Countour interval: (a), (b) $1. \times 10^{-5}$ and (c)–(f) 0.1×10^{-5}.

seasonal variability) with most of the values clustering around 5 cm s^{-1}, and higher values at both the eastern and western end of the path. Taking these velocities as transport velocity at their respective location, a water parcel would cover this stretch of 6000 km within 3 to 4 yr and thus account for the temporal evolution of sensitivities. This mechanism is consistent with the propagating signal found by Shina et al. (2004) in coupled models but has not been detected in any observational dataset so far.

Sensitivities of J_{SST} [definition (2) of the response function] with respect to temperature perturbations at 300 m (not shown) are merely distinguishable from those shown in Fig. 1: they show exactly the same evolution for year -1 to year -6.

When we turn our attention to sensitivities at the surface (Fig. 2), we find that qualitatively the patterns match those of sensitivities w.r.t. 300-m temperature (Fig. 1). However, the amplitudes are one order of magnitude less. The reason for this is the rapid damping of any temperature perturbation at the surface by heat flux on a time scale of 2–3 months, as shown, for example, by Frankignoul (1985). If we take a closer look and resolve the evolution of sensitivities seasonally, differences between surface and subsurface are apparent for the summer months but all but vanish in the winter months. Figure 3a shows the spatially integrated sensitivity of J_{T300} w.r.t. temperature for years -1 to -6, from right to left, for three different model layers, and Fig. 3b shows the same diagnostic of J_{SST}. In winter, sensitivities are almost identical throughout the water column, but they decrease rapidly in autumn (going backward in time) for the surface and also for the 50-m layer. During summer they are virtually zero. The previous spring then shows an almost instantaneous increase of the values, almost reaching the levels of the deeper layer within the main thermocline.

These results can be understood in terms of the reemergence mechanism, which was initially suggested by Namias and Born (1970) and discussed for various ocean regions by Deser et al. (2003), Alexander et al. (1999), and Alexander and Deser (1995). In a forward framework, in winter information from the atmospheric forcing is more or less equally distributed over the deep homogeneous mixed layer. During late spring and summer deeper layers are shielded from direct atmospheric forcing by a shallow mixed layer and lose only a little of their characteristics by internal mixing. Successive reentrainment of these water masses in autumn communicates this information back to the surface layers of the ocean.

This sequestering process is very effective over the time scale of 3 yr (Figs. 3a,b), the time it takes the sensitivities to travel across the Atlantic. And although there is an exponential drop-off after that, it still delivers information seven years prior to the time period when the actual scalar function J_{T300} or J_{SST} is calculated.

The comparison of sensitivities of J_{T300} and J_{SST} suggests that this mechanism provides a very effective memory system for SST perturbations despite the damping at the surface. It underlines the role of subsurface layers as memory keeper of surface conditions, communicating with the surface through the deep winter mixed layer. Thus for the remainder of this manuscript we will discuss sensitivities with respect to J_{SST}, unless otherwise mentioned.

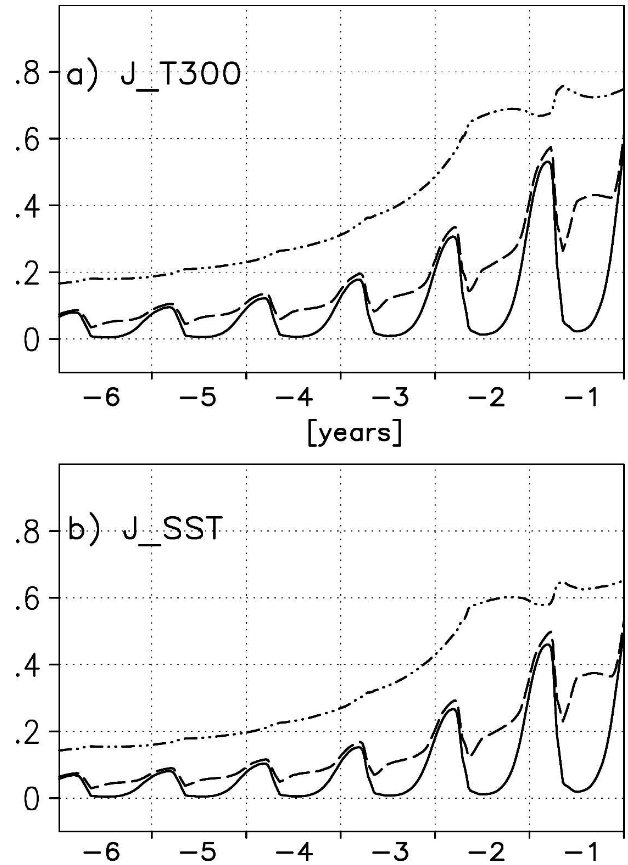

FIG. 3. Spatial average over the North Atlantic north of the equator of sensitivity of (a) J_{T300} and (b) J_{SST} w.r.t. temperature at three different levels: surface (solid), 50 m (dashed), and 300 m (dotted–dashed) for the whole integration/adjoint derivation period. Time sequence from right to left denotes years prior to the calculation of J. Units are 10^{-5} (°C °C^{-1}).

One further aspect we want to mention here is the spatial spread of sensitivities (Figs. 1 and 2), which reflects an envelope of time scales involved. If we focus on the area of *maximum* sensitivity—we might call it *center of mass*—at any one time period, then we might argue that once the temperature anomalies are created, their advection by the mean current accounts for the time scale of three to four years with which these *maximum* sensitivities propagate across the North Atlantic basin. But the spread of the sensitivities two years and more prior to the calculation of J_{SST} encloses large parts of the northern North Atlantic that cannot be explained by a single advection time scale: a whole

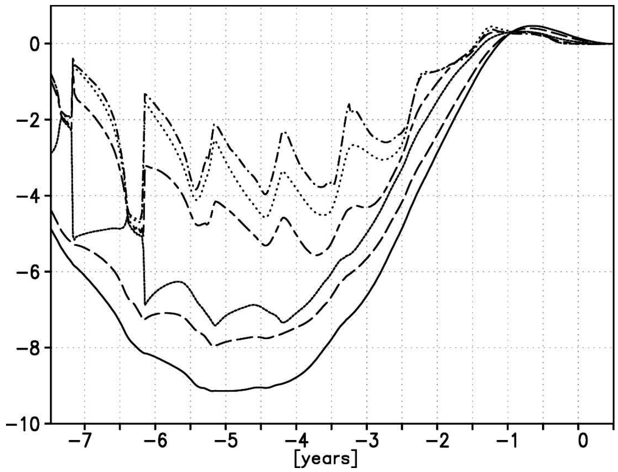

FIG. 4. Sensitivity of J_{SST} to temperature at 60°N, 55°W at various depths: time is in years *prior* to the calculation of J_{SST}, running from right to left. Depths are 2100 (solid), 1500 (long-dashed), 660 (short-dashed), 300 (long–short-dashed), 100 (dotted) and 35 m (dotted–dashed). Units are 10^{-6} (°C °C^{-1}).

range of time scales and hence mechanisms is involved in creating temperature perturbations in the eastern North Atlantic.

Referring to Figs. 1 and 2, we can identify negative sensitivities both within the thermocline and at the surface that become apparent in year −3 north of the positive temperature sensitivities along the Gulf Stream path (Figs. 2c and 1c). From this region they travel north, reach the South Greenland tip and develop into a boomerang shape with one wing etching up into the Labrador Sea to the northwest and the other wing extending into the Irminger Sea and beyond to the northeast, upstream the East Greenland Current (Figs. 2d–f and 1d–f). By year −6 negative sensitivities of J_{SST} to temperature perturbations fill the entire subpolar gyre, including the target region where J_{SST} is calculated at the end of the integration period (year 0).

The temporal evolution of sensitivity to temperature perturbations in the Labrador Sea is shown in Fig. 4 for different levels, in the upper 2000 m of the water column. The first inklings of this negative signal arrive in the Labrador Sea around years −2 to −3 prior to the calculation of J_{SST}, and the maximum negative sensitivity is reached by year −5, most noticeable in intermediate layers between 800 and 2000 m. Prior to that, the signal slowly weakens again.

The seasonal signal of Labrador Sea convection is very clear: in the surface layers sensitivity to temperature perturbations is small during summer, but in winter months perturbations play a role, with maximum impact toward the end of winter. This is the time when winter convection in the Labrador Sea is most vigorous. Thus, these characteristics suggest that the response function J_{SST} is sensitive to perturbations of convective activity in the Labrador Sea 5 yr earlier. Positive temperature perturbations at the surface stabilize the water column while negative temperature perturbations destabilize the water column and thus enhance convection. Thus, negative sensitivities seen in the surface layers suggest that enhanced convection influences surface temperatures in the eastern North Atlantic positively on a multiannual to decadal time scale.

This is a most interesting result. The background state we employ for the adjoint calculation does not exhibit significant interannual variability in the strength of convection that could precondition the development of this sensitivity pattern in the subpolar gyre. Nonetheless, the adjoint calculation singles out temperature (and salinity; not shown) and hence density in the Labrador Sea (and also the Irminger Sea) as the second important water mass and region next to the Gulf Stream advection.

Temperature perturbations can play a role via their effect on density and hence the pressure gradient, leading to velocity perturbations. However, if these temperature perturbations are compensated by concurring changes in salinity, no effects on the circulation will ensue. To conceptually separate these two aspects of thermal perturbations one might tag these with "dynamic" and "kinematic" (Marotzke et al. 1999). Sensitivities with respect to temperature and salinity are related via the thermal expansion (α) and saline contraction coefficient (β):

$$\alpha \equiv -\frac{1}{\rho}\left(\frac{\partial \rho}{\partial T}\right)_S, \quad \beta \equiv -\frac{1}{\rho}\left(\frac{\partial \rho}{\partial S}\right)_T.$$

If we denote the scalar function J_{SST} as a function of temperature T and density $\rho(T, S)$, with S being salinity,

$$J_{SST} = J_{SST}[T, \rho(T, S)], \tag{3}$$

conceptually we separate the effect of density changes that entail dynamical changes on the one hand, and the effect of salinity-compensated temperature changes on a (neutral) density surface, that are dynamically inactive, on the other hand. The sensitivity of the response function J_{SST} can therefore be expressed as

$$\begin{aligned}\left(\frac{\partial J_{SST}}{\partial T}\right)_S &= \left(\frac{\partial J_{SST}}{\partial \rho}\right)_T\left(\frac{\partial \rho}{\partial T}\right)_S + \left(\frac{\partial J_{SST}}{\partial T}\right)_\rho \\ &= -\alpha\rho\left(\frac{\partial J_{SST}}{\partial \rho}\right)_T + \left(\frac{\partial J_{SST}}{\partial T}\right)_\rho,\end{aligned} \tag{4}$$

with the first term on the rhs of Eq. (4) denoting the dynamically relevant part of the sensitivity, "dynamic sensitivity," and the second term qualifying the "kinematic sensitivity." We need to specify those two expressions in terms of the variables the adjoint calculation can provide, that is, $(\partial J_{\mathrm{SST}}/\partial T)_S$ and $(\partial J_{\mathrm{SST}}/\partial S)_T$. The sensitivity of J_{SST} w.r.t. salinity perturbations can be reformulated as

$$\left(\frac{\partial J_{\mathrm{SST}}}{\partial S}\right)_T = \left(\frac{\partial J_{\mathrm{SST}}}{\partial \rho}\right)_T \left(\frac{\partial \rho}{\partial S}\right)_T = \beta\rho\left(\frac{\partial J_{\mathrm{SST}}}{\partial \rho}\right)_T. \quad (5)$$

Substituting Eq. (5) into the first term of the rhs of Eq. (4) leads to the following representations of dynamic and kinematic sensitivity in terms of the gradients calculated by the adjoint:

(a) dynamic sensitivity, that is, with effect on circulation

$$-\alpha\rho\left(\frac{\partial J_{\mathrm{SST}}}{\partial \rho}\right)_T = -\frac{\alpha}{\beta}\left(\frac{\partial J_{\mathrm{SST}}}{\partial S}\right)_T \quad (6)$$

and (b) kinematic sensitivity, that is, no effect on circulation

$$\left(\frac{\partial J_{\mathrm{SST}}}{\partial T}\right)_\rho = \left(\frac{\partial J_{\mathrm{SST}}}{\partial T}\right)_S + \frac{\alpha}{\beta} = \left(\frac{\partial J_{\mathrm{SST}}}{\partial S}\right)_T. \quad (7)$$

Figure 5 shows dynamic (first row) and kinematic (second row) sensitivities at 300 m at the time periods of winter of year −3 (first column), winter of year −2 (second column), and winter of year −1 (third column). In year −1 the strongest signal is clearly in the kinematic sensitivity along the North Atlantic Current (Fig. 5f) with the maximum sensitivity around 50°N, 30°W. The pattern and the sign are reminiscent of the annual mean sensitivity of J_{SST} w.r.t. temperature at 300-m depth (Fig. 1a). However, at the same time dynamic sensitivities are also at work and are characterized by a dipolar pattern with strongest gradients in the same area as the maximum kinematic sensitivities.

One year earlier (year −2), the location of the center of action has shifted toward Newfoundland, and the main monopolar kinematic center (Fig. 5e) as well as the strongest gradient in the dipolar dynamical pattern (Fig. 5b) are found around 45°N, 35°W. Deeper in the thermocline the dynamic sensitivities are twice as strong as the kinematic sensitivities in both years −1 and −2 (not shown). One year prior to that, the main dynamic dipolar signal is found at the southern exit of the Labrador Sea, while the main kinematic signal lies farther south and west (not visible in the figure).

The causal chain we can derive from these results starts with positive (negative) perturbations of convection in the Labrador Sea, which thickens (thins) the Labrador Sea Water layer. Advection of this signal, first to the south and once it has reached the NAC along the northern flank of the NAC, leads to positive (negative) perturbations of the pressure gradient that are responsible for the advection of heat across the North Atlantic. Hence it leads to a strengthening (weakening) of the NAC, along which heat is transported into the eastern North Atlantic, and eventually to an increase (decrease) in SST in the target area.

The initial appearance of negative sensitivities in the target area is also connected to the buoyancy in the water column of the target area at the beginning of the adjoint calculation period: cold temperature anomalies beneath the local mixed layer contribute to a higher density of the water below and therefore stabilize the water column, thus inhibiting a deeper mixing with an ensuing cooling of the well-mixed column. The local model mixed layer depth in winter in the northeast Atlantic is about 400 to 500 m and thus below the threshold that is used for the calculation of both J_{SST} and J_{T300}. In the adjoint calculations we find that sensitivities below the depth used for the calculation of J_{T300} are negative, suggesting that the mechanism described above is at work. If we resort again to the partition of sensitivities into kinematic and dynamic (Fig. 6), then we find that (positive) kinematic sensitivities (shaded in Fig. 6) are mostly confined to the column of the winter mixed layer and weaker negative dynamic sensitivities (contours in Fig. 6) dominate below this region, thus supporting the explanation given above for the initial development of negative sensitivities in lower layers in the target area.

As the definition of J_{SST} as well as J_{T300} is steplike in the vertical, our suspicion was that this buoyancy-related sensitivity is an artificial effect of these definitions. To avoid the artificial dipole in the definition we also conducted an additional adjoint calculation, where the response function J_{T300} was modified by a weighting function w_k in the vertical with $w_k = 1$ for model layers k with depth $z_k <= 300$ m, and w_k decaying exponentially below that depth. We found, however, that the results are virtually identical to the J_{T300} experiment, and negative sensitivities develop horizontally and vertically in much the same fashion (not shown).

To sum up, negative perturbations of temperatures in the Labrador Sea and Irminger Sea lead to positive sea surface temperature perturbations in the eastern North Atlantic 5 to 6 yr later. The effect of these perturbations in the Labrador and Irminger Seas is a combination of (a) perturbations that become dynamically important 2 to 3 yr later in the main pycnocline, once they reach the Gulf Stream/NAC system, and (b) thermodynamical stabilization of the water column in the target area. We

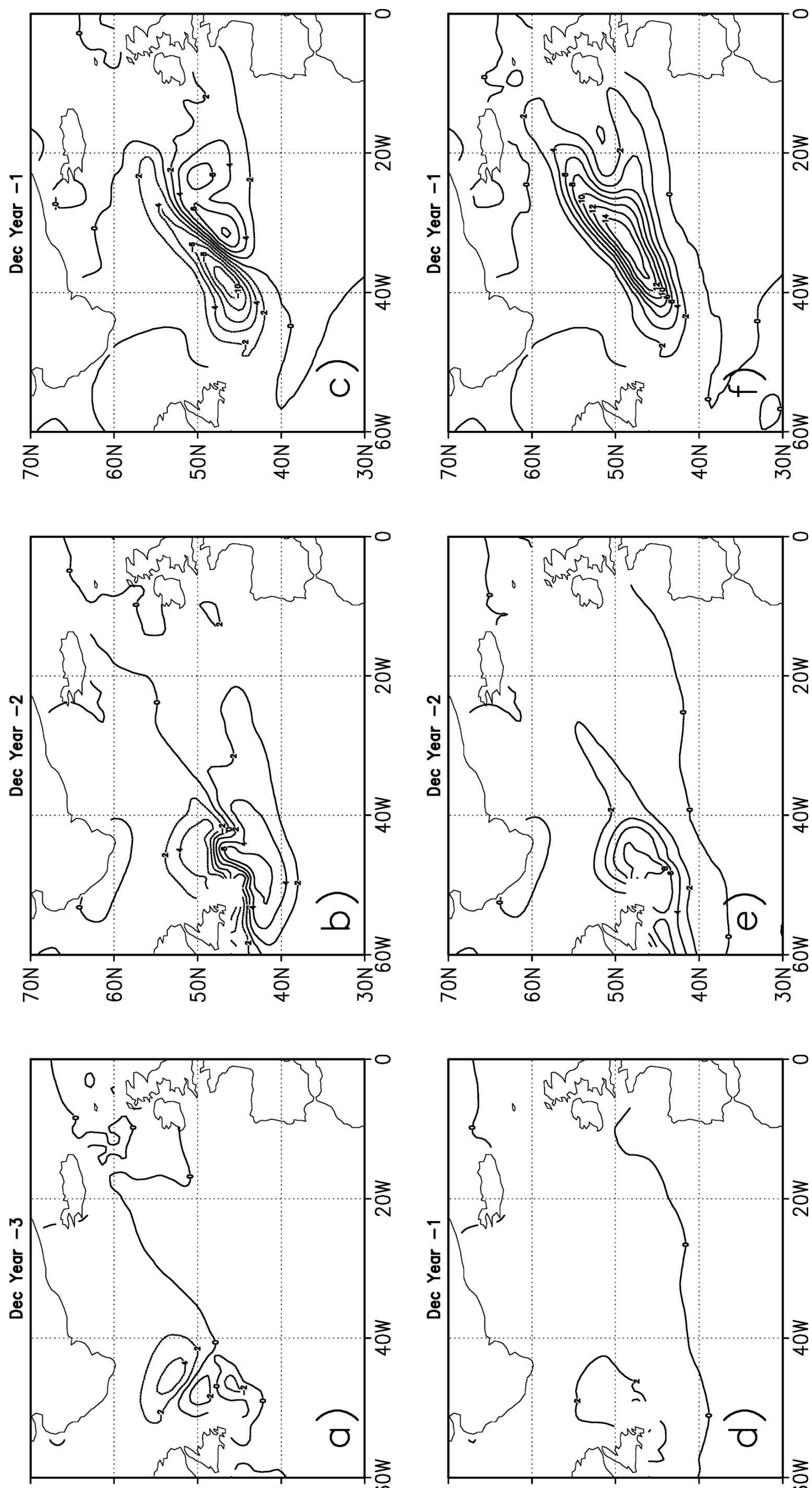

FIG. 5. Sensitivity of J_{SST} to temperature at 300-m depth split up into (a)–(c) dynamic and (d)–(f) kinematic sensitivities (for explanation of dynamic and kinematic sensitivities see text). Time periods are Decembers of years (a), (d) −3, (b), (e) −2, and (c), (f) −1. Units are 10^{-5} (°C °C^{-1}).

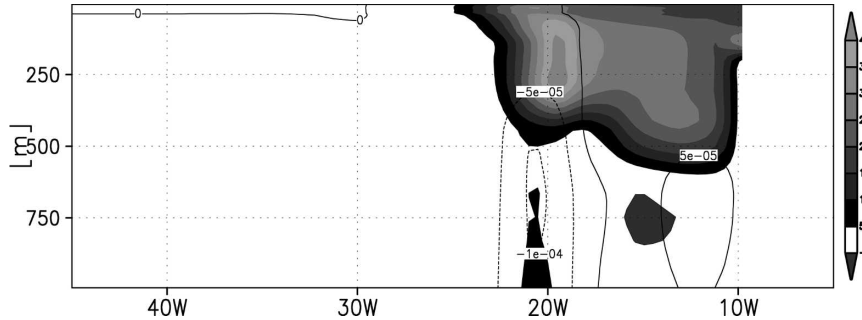

FIG. 6. Vertical section of kinematic (gray color shading) and dynamic sensitivities (contours) at 55°N at the end of November in year 0. Units: (°C °C^{-1}).

can only speculate at this point about the relevance of these processes in nature, but it has been established in various investigations, for example, by Curry and McCartney (2001), Cooper and Gordon (2002), and Talley and McCartney (1982), that strong Labrador Sea convection and the accompanying local temperature decrease result in a Labrador Sea Water thickening and propagation of the signal along the Gulf Stream extension and the NAC into the eastern part of the northern North Atlantic.

The time scale of the signal spreading appears to be quite realistic. Sy et al. (1997) demonstrated the fast spreading of newly formed intermediate waters in the Labrador Sea across the North Atlantic within 4 to 5.5 yr. Very similar estimates, roughly 6 yr, have been put forward by Curry and McCartney (2001), and these values are consistent with results by Cooper and Gordon (2002) derived from the analysis of coupled model experiments with the HadCM3.

The order of magnitude of these sensitivities in the Labrador and Irminger Seas is the same as we have seen in the advective signal in the upper part of the water column along the Gulf Stream path, so they are equally important for the heat budget in the eastern parts of the North Atlantic but exert their influence on different time scales.

b. Tropical and subtropical precursors

Figure 7a shows a time series of sensitivity of J_{SST} to surface temperature at 35°N, 75°W in the Gulf Stream area. It is evident that the signal attains its maximum in this region about two years prior to the calculation of J_{SST} in year 0, but clearly also in the preceeding years −3, −4, and −5, a winter time peak of sensitivity is apparent. Although lower, these peak values are still of the same order of magnitude as the maximum peak in winter of year −3. These multiple peaks demonstrate the spread of time scales involved in advection along the NAC that was already visible in Figs. 1 and 2, but the multiyear persistence of these sensitivities is provided by the thermocline waters in this area. Figure 7b displays the time evolution of the same surface temperature sensitivity at 35°N together with sensitivity to thermocline temperatures at 300 and 660 m. Clearly visible is the onset of sensitivity rise at a time scale of 2 yr. It reaches its maximum after three to four years, depending on depth, and decays slowly for several years.

As can be seen from Fig. 7b sensitivities in the Gulf Stream region persist for several years. In the natural world, SST anomalies in the Gulf Stream region on the interannual time scale are likely to be forced by NAO-related heat flux and wind stress (Deser and Blackmon 1993). The multiannual time scale is thus conceivable with years of positive (negative) NAO winters clustering and thus producing a series of winters of positive

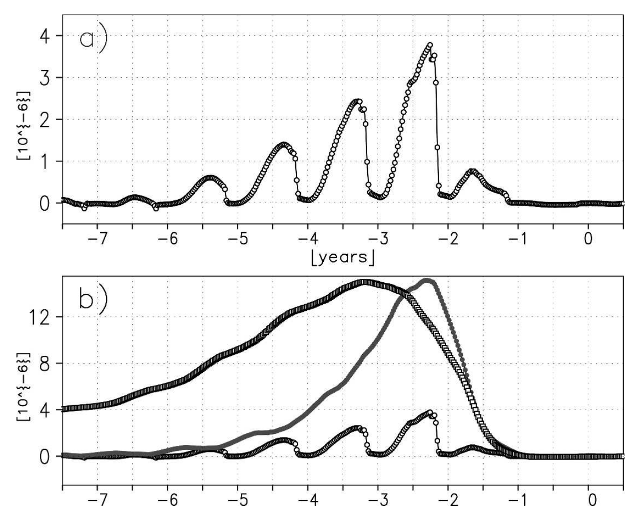

FIG. 7. Sensitivity of J_{SST} to sea surface temperature at 35°N, 75°W in the Gulf Stream region. Time is running back from right (year 0) to left (year −7) prior to the calculation of J_{SST}: (a) sensitivity to SST, and (b) sensitvity to SST (open circles), temperature at 300 m (filled circles), and temperature at 660 m (open boxes). Note the different scale in (a) and (b).

(negative) SST anomalies in this area, one of the centers of the SST tripole. However, in the model experiments performed here, the climatological forcing does not produce this type of interannual variations, so we have to look for precursors of this persistent feature in the ocean.

When we trace the sensitivity in the area off the United States further back in time, we can identify essentially two—direct—source regions: the subtropical gyre to the east and the tropical/subtropical region to the south. In the following we will explore these two regions that are connected to these sensitivities through different pathways: (i) the upper subtropical North Atlantic that is mainly goverened by the wind-driven dynamics of the *ventilated thermocline* (Luyten et al. 1983) and (ii) the equatorial/tropical Atlantic with its swift equatorial current system communicating with the Gulf Stream via the North Brazil Current.

1) Subtropical precursors

Returning to Fig. 1f we see that in year −6 the largest sensitivities at 300-m depth, apart from those in the subpolar gyre, are present in the western half of the subtropical gyre between 60° and 40°W, around the latitude band from 15° to 35°N. This organized sensitivity area travels from east to west between year −6 and year −3 (Figs. 1f–c, in reversed order), until it feeds into the Gulf Stream around year −3, the time of highest sensitivities in Fig. 7. The characteristics of its evolution suggest advection of temperature anomalies by mean ocean currents in the subtropical gyre.

Dynamically, these sensitivities can be understood in terms of the wind-driven circulation in the ventilated thermocline. Temperature perturbations in the southern subtropical gyre are advected to the west along density or neutral surfaces by the mean current and eventually feed into the Gulf Stream.

The density surface through which the 300-m horizon cuts in this region between 40° and 70°W is the σ_θ = 26.0 surface that is ventilated near 30° to 35°N, around 40°W, in the eastern North Atlantic basin. To gain a picture of sensitivity on density surfaces, climatological winter potential temperature and salinity from the control integration have been used to calculate potential density σ_θ according to Fofonoff and Millard (1983). The depth of potential density surfaces between σ_θ = 24.0 and σ_θ = 27.0 with σ_θ = 0.2 intervals has been calculated as follows: for a particular density surface σ_θ and a particular model grid point, the potential density of all model layers is compared to σ_θ to determine with which of the model z layers the surface intersects. Applying this procedure at each grid point yields the depth of the σ_θ surface and the corresponding model layer index. The latter is used to construct the sensitivity patterns on the different σ_θ levels. The results are shown in Fig. 8, for the sequence of winters of years −3 (Fig. 8b), −4 (Fig. 8c), −5 (Fig. 8d), and −6 (Fig. 8e) prior to the calculation of J_{SST}.

Figure 8a displays the climatological depth of the layer. It is characterized by the typical bowl shape of subtropical density surfaces and a concentration of isolines to the northeast of the bowl: this area between 40° and 50°W in the latitude band 35°–40°N can be considered as the ventilation region where most of the water masses enter this surface through Ekman pumping in winter.

The sensitivity blob we see in Fig. 8e (year −6) around 30°N is close to the ventilation region of this layer. The sensitivity in winter of year −5 prior to the calculation of J_{SST} (Fig. 8d) has extended farther to the west and grown slightly in amplitude. The intensification and westward movement continues until in year −3 prior to the calculation of J_{SST}, a large area of sensitivities feeds into the area where the model Gulf Stream leaves the U.S. coast. The regions that are successively passed by the sensitivities make up the bowl of this potential density surface.

2) Tropical precursors

As far as the equatorial region is concerned, Figs. 1 and 2 seem to tell us that this area does not contribute to SST perturbations in the northeastern Atlantic. However, focusing on sensitivities in that area still provides interesting aspects. The sensitivities in the tropical region are one order of magnitude smaller than those in the subpolar and subtropical regions—hence their "nonexistence" in the large-scale picture. The main (oceanic) connection between the Gulf Stream off the American seaboard and the tropical regions is the North Brazil Current that runs along the South American coast off north Brazil.

Along this path, the time evolution of sensitivities of J_{SST} to temperature in the upper water column between latitudes 15°N and 20°S (about 3000 km apart) shows a consecutive rise of sensitivities between years −2 and −4; the farther south the respective location lies, the later the rise occurs (not shown). Analysis of this signal shows that their spatial evolution—somewhat counterintuitively—is not primarily due to advection of temperature perturbations.

These sensitivities can be traced to the east across the tropical ocean basin, and the excitation of the signals appears to be tied to the seasonal cycle: high sensitivities around 40°–50°W in consecutive years always ap-

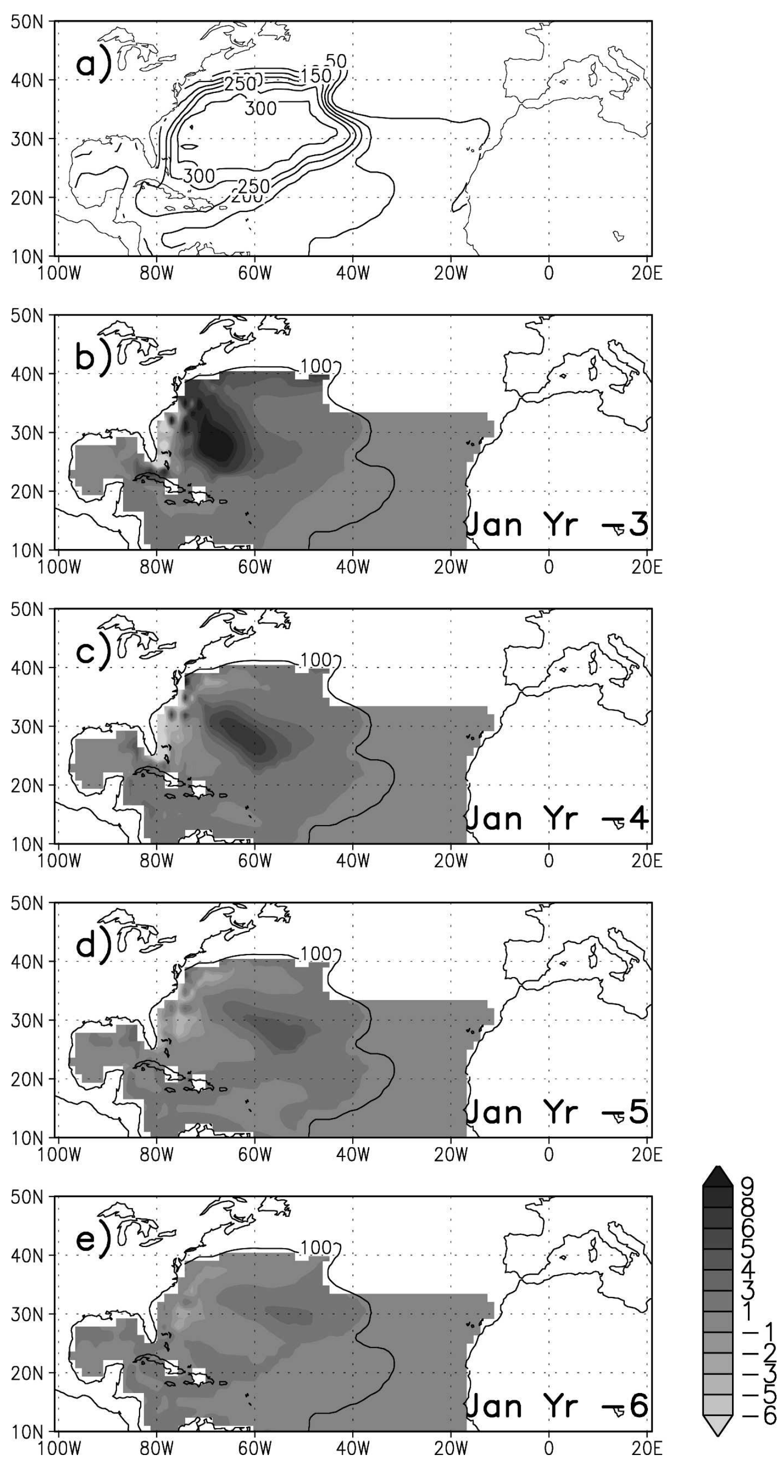

FIG. 8. (b)–(e) Sensitivity of J_{SST} w.r.t. temperature on potential density surface $\sigma_\theta = 26$ for years -3 to -6 prior to the calculation of J_{SST}. Countour interval: 10^{-6} (°C °C^{-1}). (a) The climatological depth of the midpoint of this surface. CI: 50 m. Additionaly, in (b)–(e), the climatological 100-m depth contour of this surface is drawn for reference.

pear in late autumn/early winter. This is an indication that the interplay of atmospheric forcing and ocean dynamics is important in this region.

These sensitivities are small—one order of magnitude less than the subtropical and subpolar signals—and do not actually provide particularly strong forcing and preconditioning of northeastern North Atlantic SSTs. However, dynamics in particular in the Tropics can only be understood if we consider the coupled ocean–atmosphere system and possible positive feedbacks. This interaction is not included in the model setup, and thus the atmospheric bridge between the Tropics and midlatitudes cannot show in these sensitivities. Nonetheless, sensitivities to velocity and wind stress perturbations lead us to suspect that the full system including tropical ocean–atmosphere interactions can well lead to an amplification of sensitivities in the Tropics. Such an investigation requires the adjoint of a (hybrid) coupled model, which is beyond the scope of this paper.

4. Discussion

As indicated at the beginning of this investigation, the purpose of the experiment design is to reveal which quantities influence SST and heat content in the eastern North Atlantic: what is their spatial extent, what is their spatial evolution, which are the relevant time scales, and how do different processes work together to make up what we observe in the northeastern corner of the North Atlantic. So what have we understood in terms of the relative importance of mechanisms, the influence of remote areas such as the Labrador Sea, the subtropics, and the Tropics, and the seasonality of the signals?

Let us start with the latter: the long-term memory of SST can only be sustained by the internal ocean. For the ocean to provide a memory of surface conditions the seasonal cycle is important. Only during times of deep surface mixed layers can the connection between surface and interior ocean be established. For the characteristics of water masses to be preserved a mechanism by which they are shielded from damping surface fluxes is provided by the thin summer mixed layer. The nearly vanishing sensitivities in summer indicate that only heat flux forcing in winter, when the mixed layer is deep and provides a pathway to the permanent thermocline, is relevant for the ocean's long-term memory.

The knowledge of this reemergence process is well established, but it has preferentially been thought of in terms of a *local* mechanism to prolong memory beyond the seasonal damping time scale, defining it mainly for areas of weak flows (Timlin et al. 2002). This, however, is a rather static picture of the upper ocean. As we have seen here, the reentrainment of temperature anomalies at position y, produced in one winter at an upstream position x, can be followed not only in time but also in space. This is to say the Lagrangian view of reemergence seems more appropriate to capture the volume of reemergence, particularly in regions of strong flows.

This brings us to the relative role of different mechanisms: advection of temperature perturbations by the climatological currents along the Gulf Stream and the NAC is the dominant mechanism on the interannual (2–4 yr) time scale. The spatial patterns of sensitivity are very similar to lag-correlation results by Sutton and Allen (1997), for example. However, the movement of the signal is much faster than their 7–9-yr time scale. Though Shina et al. (2004) have found similar propagation features on the interannual time scale in a coupled ocean–atmosphere model integration, no such feature could be established in observational datasets, so its relevance is not clear.

In assessing the time scale we have focused on the *maximum* sensitivity at any one time period (Fig. 1). However, sensitivity is also spread over the whole northern domain of the North Atlantic after a couple of years and thus already suggests that a broad spectrum of time scales is involved.

For example, sensitivities to 5-m temperature in the winters of years -2 and -3 (Figs. 2b,c) show positive values across almost the entire width of the North Atlantic in the latitude band between 40° and 50°N. This indicates that many processes with different characteristic time scales are involved in shaping the evolution of anomalies. Also at times an out-of-phase evolution of maximum sensitivities at the surface and at 300-m depth is evident (not shown), indicating that sensitivities at the surface are advected faster than those in the thermocline, spreading information over a larger area than would be the case by information propagation only in the thermocline.

The spread of time scales brings us to the second important region, the western part of the subpolar gyre, that exerts its influence on the eastern North Atlantic on a longer time scale. These sensitivities in the subpolar gyre, most prominently in the Labrador Sea, are found to be as important as those in the NAC. Their origin, however, is "dynamical": colder, denser water masses originating in the Labrador Sea get advected into the central subpolar gyre and give rise to density gradients in the upper water column and thus to an increase of velocities, thereby increasing heat transport into the northeastern North Atlantic. This mechanism is consistent with results of Curry and McCartney

(2001) and Cooper and Gordon (2002), and is also supported by a water mass analysis by Haines and Old (2005).

From the Gulf Stream region off the U.S. seaboard sensitivities can be traced into the ventilated thermocline of the subtropical gyre, on the one hand, and farther to the south into the tropical regions on the other hand. In the subtropical gyre the circulation from the respective ventilation region of an isopycnal layer to the return flow through the western boundary current has the potential to influence the eastern North Atlantic on a longer time scale. The geographical location of the ventilation region, the length of the flow path, and velocities along that path vary from isopycnal layer to isopycnal layer, and thus a wide range of time scales is involved (Fig. 7b).

Sensitivities in the tropical regions are small and perturbations there seem to be no major players for North Atlantic SST. Apart from the magnitude, characteristics of the sensitivity patterns indicate that propagation of perturbations from east to west is dynamically important and that the seasonality of the signal plays a role in connection with the surface forcing. It has yet to be investigated if in a coupled system these sensitivities are amplified through positive feedback mechanisms.

In numerical model integrations Grötzner et al. (1998) and Wu and Liu (2005) have analyzed a coupled ocean–atmosphere mode in the midlatitude North Atlantic that operates on the decadal time scale (17 yr in the first case, 12–16 yr in the latter). These studies strongly suggest that SST variations on the decadal time scale are due to ocean–atmosphere feedbacks. Thus, one of the major drawbacks of our study is certainly the "one-way" approach: climatological atmospheric fluxes force the ocean and no feedback of ocean surface conditions to the atmospheric state can be imparted here. As we have seen, tracing back temperature perturbations from the northern North Atlantic to the Tropics is possible, and the next step is certainly to use a coupled adjoint model to investigate these sensitivities in depth. This work is under way (S. Osprey 2005, personal communication), and the results of the experiments with the uncoupled model can serve as a benchmark for the coupled experiments.

In nature, in the Gulf Stream extension nonlinear dynamics provide the means of mixing the cold and warm water masses that meet there, while in the model these processes are parameterized by eddy viscosity. Whether this representation has a major influence on the way perturbations are propagated is unclear.

Acknowledgments. The Deutsche Forschungsgemeinschaft, Bonn, Germany, supported this study through the Sonderforschungsbereich 512: Tiefdruckgebiete und Klimasystem des Nordatlantiks.

REFERENCES

Alexander, M. A., and C. Deser, 1995: A mechanism for the recurrence of wintertime SST anomalies. *J. Phys. Oceanogr.,* **25,** 122–137.

——, ——, and M. S. Timlin, 1999: The reemergence of SST anomalies in the North Pacific. *J. Climate,* **12,** 2419–2433.

Cooper, C., and C. Gordon, 2002: North Atlantic oceanic decadal variability in the Hadley Centre Coupled Model. *J. Climate,* **15,** 45–72.

Curry, R., and M. McCartney, 2001: Ocean gyre circulation changes associated with the North Atlantic Oscillation. *J. Phys. Oceanogr.,* **31,** 3374–3400.

Czaja, A., and C. Frankignoul, 1999: Influence of the North Atlantic SST on the atmospheric circulation. *Geophys. Res. Lett.,* **26,** 2969–2972.

Deser, C., and M. Blackmon, 1993: Surface climate variations over the North Atlantic Ocean during winter. *J. Climate,* **6,** 1743–1753.

——, M. A. Alexander, and M. Timlin, 2003: Understanding the persistence of sea surface temperatures in midlatitutdes. *J. Climate,* **16,** 57–72.

Errico, R. M., 1997: What is an adjoint model? *Bull. Amer. Meteor. Soc.,* **78,** 2576–2591.

Esbensen, S. K., and Y. Kushnir, 1981: The heat budget of the global ocean: An atlas based on estimates from surface marine observations. Climatic Research Institution Tech. Rep. 29, Oregon State University, 244 pp.

Fofonoff, N. P., and R. C. Millard Jr., 1983: Algorithms for computation of fundamental properties of seawater. Unesco Tech. Rep. 44, 58 pp.

Fraedrich, K., and R. Blender, 2003: Scaling of atmosphere and ocean temperature correlations in observations and climate models. *Phys. Rev. Lett.,* **90,** 108501, doi:10.1103/PhysRevLett90.108501.

——, U. Luksch, and R. Blender, 2004: 1/*f* model for long-time memory of the ocean surface temperature. *Phys. Rev. E.,* **70,** 037301 doi:10.1103/PhysRevE.70.037301.

Frankignoul, C., 1985: Sea surface temperature anomalies, planetary waves and air–sea feedback in the middle latitudes. *Rev. Geophys.,* **23,** 357–390.

——, P. Müller, and E. Zorita, 1997: A simple model of decadal response of the ocean to stochastic wind stress forcing. *J. Phys. Oceanogr.,* **27,** 1533–1546.

Grötzner, A., M. Latif, and T. P. Barnett, 1998: A decadal climate cycle in the North Atlantic Ocean as simulated by the ECHO coupled GCM. *J. Climate,* **11,** 831–847.

Haines, K., and M. Old, 2005: Diagnosing natural variability of North Atlantic water masses in HadCM3. *J. Climate,* **18,** 1925–1941.

Hansen, D. V., and H. F. Bezdek, 1996: On the nature of decadal anomalies in the north Atlantic sea surface temperature. *J. Geophys. Res.,* **101,** 8749–8758.

Hellermann, S., and M. Rosenstein, 1983: Normal monthly wind stress over the world ocean with error estimates. *J. Phys. Oceanogr.,* **13,** 1093–1104.

Jaeger, L., 1976: Monatskarten des Niederschlags für die ganze Erde. Bericht des Deutschen Wetterdientes, Vol. 139, Offenbach, Germany, 33 pp.

Junge, M. M., and T. W. N. Haine, 2001: Mechanisms of North

Atlantic wintertime sea surface temperature anomalies. *J. Climate,* **14,** 4560–4572.

Krahmann, G., M. Visbeck, and G. Riverdin, 2001: Formation and propagation of temperature anomalies along the North Atlantic current. *J. Phys. Oceanogr.,* **31,** 1287–1303.

Levitus, S., 1982: *Climatological Atlas of the World Ocean.* NOAA Prof. Paper 13, 173 pp.

Luyten, J. R., J. Pedlosky, and H. Stommel, 1983: The ventilated thermocline. *J. Phys. Oceanogr.,* **13,** 292–309.

Marotzke, J., R. Giering, K. Q. Zhang, D. Stammer, C. Hill, and T. Lee, 1999: Construction of the adjoint MIT ocean general circulation model and application to Atlantic heat transport sensitivity. *J. Geophys. Res.,* **104,** 29 529–29 548.

Marshall, J., and Coauthors, 2001: North Atlantic climate variability: Phenomena, impacts and mechanisms. *Int. J. Climatol.,* **21,** 1863–1898.

Namias, J., and R. M. Born, 1970: Temporal coherence in the North Pacific sea surface temperature patterns. *J. Geophys. Res.,* **75,** 5952–5955.

Shina, B., B. Topliss, and J. Harle, 2004: Eastward propagating surface anomalies at ocean gyre boundaries. *J. Geophys. Res.,* **109,** C12005, doi:10.1029/2004JC002393.

Sutton, R. T., and M. R. Allen, 1997: Decadal predictability of North Atlantic sea surface temperature and climate. *Nature,* **388,** 563–567.

Sy, A., M. Rhein, J. R. N. Lazier, K. P. Koltermann, J. Meinke, A. Putzka, and M. Bersch, 1997: Surprisingly rapid spreading of newly formed intermediate waters across the North Atlantic Ocean. *Nature,* **386,** 675–679.

Talley, L. D., and M. S. McCartney, 1982: Distribution and circulation of Labrador Sea Water. *J. Phys. Oceanogr.,* **12,** 1189–1205.

Timlin, M. S., M. A. Alexander, and C. Deser, 2002: On the reemergence of North Atlantic SST anomalies. *J. Climate,* **15,** 2707–2712.

Wolff, J.-O., E. Maier-Reimer, and S. Legutke, 1997: The Hamburg Ocean Primitive Equation Model HOPE. DKRZ Tech. Rep. 13, 103 pp.

Wu, L., and Z. Liu, 2005: North Atlantic decadal variability: Air–sea coupling, oceanic memory and potential Northern Hemisphere resonance. *J. Climate,* **18,** 331–349.